Journal of Electronic Materials (2023) 52:7325–7336
https://doi.org/10.1007/s11664-023-10636-y

ORIGINAL RESEARCH ARTICLE

Energy Conversion Performance and Optimization of Wearable Annular Thermoelectric Generators

Chenchen Guo[1] · Aibing Zhang[1] · Dandan Pang[2] · Jianhua Cao[3]

Received: 30 April 2023 / Accepted: 21 July 2023 / Published online: 23 August 2023

Abstract

This paper presents a theoretical model for a human skin-wearable annular thermoelectric generator (WATEG) system and provides analytical solutions for its energy conversion performance. The Pennes equation is used to model the heat transfer of human skin, which is assumed to be a cylindrical multilayer structure composed of subcutis, dermis, and epidermis. The heat exchanges induced by blood perfusion and metabolic heat generation within the skin tissue are taken into account. It is found that the influence of skin effect and contact thermal resistance between the human skin and flexible substrate plays a significant role in the energy conversion performance of the WATEG and should be considered. The matched load resistance, optimal fill factor, and height of thermoelectric legs are determined through numerical analysis. The findings of this study can be applied to the practical design of WATEG devices and are expected to contribute to their optimization.

Keywords Wearable annular thermoelectric generator · body heat harvesting · performance optimization · self-powered devices

List of Symbols

A	Area (m^2)
c	Specific heat (J/kg/K)
F	Fill factor (%)
H	Height (m) or microhardness (MPa)
h	Convection coefficient or contact thermal conductance ($W/m^2/K$)
I	Current (A)
j	Current density (A/m^2)
K	Thermal conductance (W/K)
P	Power output ($\mu W/cm^2$) or contact pressure (kPa)
Q	Heat flux (W)
q	Heat flux density (W/m^2)
R	Electric resistance (Ω)
r	Radius (mm)
T	Temperature (K)

Greek Letters

α	Seebeck coefficient (V/K)
Δa	Asperity slope (rad)
δ	Thicknesses (mm)
θ	Angle (rad)
ε	Surface roughness (μm)
ρ	Density (kg/m^3)
σ	Electric conductivity (S/m)
λ	Thermal conductivity (W/m/K)
ω	Blood perfusion rate (mL/mL/s)

Subscripts

a	Ambient environment
b	Blood
c	Contact interface
d	Dermis
e	Epidermis
eff	Effective property
en	Encapsulation layer
f	Convection at heat sink
fm	Fill material
i	i-th layer

✉ Aibing Zhang
zhangaibing@nbu.edu.cn

✉ Dandan Pang
pangdandan@hncj.edu.cn

[1] School of Mechanical Engineering and Mechanics, Ningbo University, Ningbo 315211, People's Republic of China

[2] Henan Province Key Laboratory of Water Pollution Control and Rehabilitation Technology, Henan University of Urban Construction, Pingdingshan 467036, People's Republic of China

[3] School of Mechanical and Electrical Engineering, Huangshan University, Huangshan 245021, People's Republic of China

m	Metabolism
n	*N*-type thermoelectric leg
out	Output
p	*P*-type thermoelectric leg
s	Body core temperature or subcutis

Abbreviations

DPL	Dual-phase-lag
TEG	Thermoelectric generator
WATEG	Wearable annular thermoelectric generator
WTEG	Wearable thermoelectric generator

Introduction

In recent years, wearable electronic devices have become extensively used in medical and health fields to monitor vital signs such as blood pressure, oxygen saturation, electromyography, and pulse using various sensors.[1,2] This real-time monitoring enables health detection on the human body and facilitates clinical applications, eliminating the need for patients to visit hospitals. However, wearable electronic devices with installed chemical batteries are inconvenient since they require frequent charging, which may interrupt data collection over long periods. Wearable thermoelectric generators (WTEGs) have gained considerable attention due to their environmental friendliness, simplicity, high reliability, lack of moving components, excellent stability, and long service life compared to chemical batteries.[3,4] By converting heat energy from the human body into electricity directly, WTEGs can achieve the wearable electronics self-powered, and provide a continuous 24-h power supply without the need for battery charging. Nevertheless, the applications of WTEGs are significantly limited due to their low power density.[5] Moreover, the energy conversion performance of WTEGs depends not only on the device configuration but also on the characteristics of the human skin in close contact with them.

The skin is the largest organ in the human body and performs crucial functions, including protecting the body and regulating its temperature. It is composed of three layers: the epidermis, dermis, and subcutis.[6] The human body generates energy through metabolism and radiates it to the environment via convection and evaporation, thereby maintaining a relatively constant core temperature.[7] The human body can be utilized as a heat source to power generation of WTEGs since there is usually a temperature gradient between the ambient temperature and the body temperature. The normal body temperature of healthy adults is approximately 37°C.[8] For precise prediction of WTEG performance and regulation of their geometrical configuration, accurate models that consider the effect of human skin are critical.[9] Wijethunge et al.[10] proposed a simplified human thermoregulatory model for the design of WTEGs, which estimated the thermal properties of human skin without rigorous calculations. The authors found that failing to consider physiological processes could result in deviations of 10–60% in the prediction of WTEG performance. Zhang et al.[11] developed a theoretical model for WTEGs using the Pennes bioheat transfer equation, and the skin tissue was modeled as a multilayer structure. They concluded that the influence of heat exchange through blood perfusion on WTEG power output should be considered, while the metabolic heat generation can be ignored. Zhang et al.[12] established an analytical model based on the dual-phase-lag (DPL) bioheat transfer theory to investigate the dynamic thermal responses of the skin-WTEG system. Their findings indicated that it would take more than 10 min to reach the thermal steady-state after a thermal perturbation imposed on the skin-WTEG system. Furthermore, they found that the classical Fourier heat transfer model could predict WTEG performance with acceptable accuracy. The temperature difference between the body and the surrounding environment serves as a stable driving force for WTEGs. However, the effectiveness of this driving force is also constrained by the ambient temperature itself. Suarez et al.[13] introduced a WTEG utilizing bulk legs and liquid metal interconnects and observed poor power output in 35°C weather due to the close proximity of the outside temperature to the skin temperature, resulting in a minimal temperature differential. To address this challenge, Jeong et al.[14] developed an innovative WTEG capable of harnessing both body heat and light as dual energy sources, providing a significantly higher driving force. Remarkably, this novel design retained 83.1% of its power output when operating at a high ambient temperature of 35°C, compared to conditions at room temperature.

Upon an examination of references,[9–14] it was observed that they exclusively focused on flat WTEGs with thermoelectric legs featuring a flat cross-sectional configuration. However, for practical applications, such as recovering body heat from the wrist, neck, lower leg, and ankle, the heat source may be considered cylindrical in shape. The use of flat WTEGs may result in low power density due to the relative geometric mismatch between the WTEG devices and human skin. To overcome this issue, wearable annular thermoelectric generators (WATEGs) with annular-shaped legs can be used to establish closer contact with the human body, thereby reducing the contact thermal resistance between the WATEG and the skin compared to flat WTEGs. Shen et al.[15] derived the fundamental equations for annular thermoelectric generators (ATEGs) based on a one-dimensional (1D) steady heat transfer model. Kaushik and Manikandan[16] investigated the impact of the Thomson effect on the energy and exergy efficiency of ATEGs, while our previous works developed general theoretical models that discussed the influence of interface layers and the configuration of

thermoelectric legs on ATEG performance.[17–19] In addition, Fan and Gao[20] established a three-dimensional (3D) numerical model to analyze the energy conversion performance and mechanical reliability of a segmented ATEG under steady-state and transient conditions. However, to the best knowledge of the authors, the issue of integrating WATEG with human skin has not yet been investigated.

In view of the above literature analysis, the purpose of this paper is to develop a theoretical model that can evaluate the energy conversion performance of WATEGs while taking into account the effect of human skin. Firstly, analytical solutions for the temperature distribution and power output of WATEGs are provided. Secondly, the influence of physiological processes within the skin tissue, including metabolic heat generation and blood perfusion as well as the geometrical configuration of thermoelectric legs and thermal boundary conditions, is studied through numerical results to gain a better understanding of the WATEG. Finally, some concluding remarks are made.

Analytical Model for the WATEG Integrated with Human Skin

The structure diagram of the WATEG integrated with human skin is shown in Fig. 1. A three-layer human skin model, consisting of subcutis, dermis, and epidermis, is adopted. The WATEG is composed of *P*- and *N*-type annular thermoelectric legs that are sandwiched between a thermally conductive flexible substrate and an encapsulation layer. Gaps between the legs are filled with a fill material of lower thermal conductivity, and a heat sink is placed on the cold side to enhance convective heat dissipation from the WATEG.

The modeling is carried out using a polar coordinate system with the origin located at the center of the human skin. The radius at the bottom surface of the subcutis is denoted as r_s. The radii at the interfaces of subcutis/dermis, dermis/epidermis, epidermis/substrate, substrate/thermoelectric legs, thermoelectric legs/encapsulation layer, and encapsulation layer/heat sink are denoted as r_d, r_e, r_c, r_1, r_2, and r_a, respectively. The corresponding temperatures at these interfaces to be determined are assumed to be T_d, T_e, T_c, T_1, T_2, and T_{en}, respectively. The influence of metallic electrodes is neglected due to their high thermal and electrical conductivity. For simplicity, it is assumed that the *P*- and *N*-type legs of the WATEG have symmetric dimensions and material properties in the subsequent theoretical analysis. Moreover, the impact of temperature-dependent physical properties of thermoelectric material on the performance of the WTEG is minimal and can be neglected when the material properties at room temperature are employed.[11,12] The angles in the direction of circumference for each *P*-type (or *N*-type) thermoelectric leg and the WATEG are θ_p and θ, respectively. The thicknesses of each leg and WATEG are denoted as δ_p and δ, respectively. The core body temperature and ambient temperature are considered as constants, denoted as T_s and T_a, respectively.

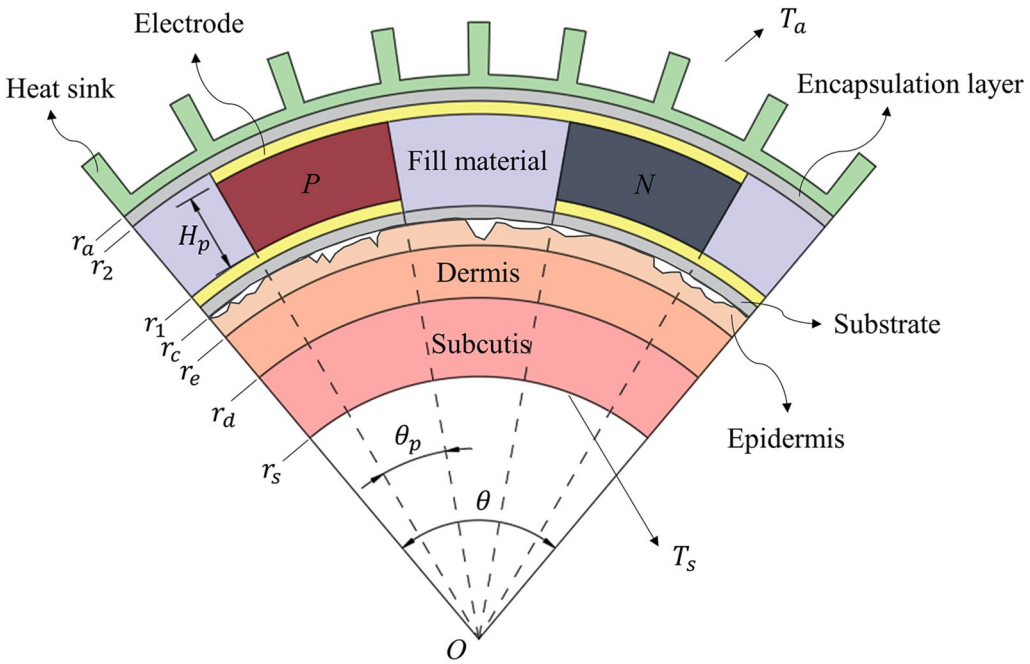

Fig. 1 The structure diagram of the WATEG integrated with human skin.

Temperature Field for Human Skin

The heat transfer of the human skin can be effectively modeled using the widely accepted Pennes equation,[21] which takes the following form:

$$\lambda\frac{\mathrm{d}^2T}{\mathrm{d}r^2}+\lambda\frac{1}{r}\frac{\mathrm{d}T}{\mathrm{d}r}-\omega_b\rho_b c_b\left(T-T_s\right)+q_m=0 \tag{1}$$

where T and λ are the temperature and thermal conductivity specific to the designated layer of skin tissue, respectively. The parameters ω_b, ρ_b, and c_b denote the perfusion rate, density, and specific heat capacity of blood, respectively. The temperature of blood is regarded as the core body temperature T_s. The term q_m represents the metabolic heat generation and is assumed to be uniformly distributed throughout the skin tissue. In Eq. 1, the first two terms represent the heat conduction, the third term represents heat exchange induced by the blood perfusion, and it only exists in the subcutis layer and dermis.

The heat flow rate $Q(r)$ within the human skin can be expressed as:

$$Q(r)=-\lambda A(r)\frac{\mathrm{d}T(r)}{\mathrm{d}r} \tag{2}$$

where $A(r)$ is the cross-sectional area at the corresponding radius of skin tissue. The solutions of the temperature field in skin tissue are obtained as:

$$T(r)=\begin{cases}B_sI_0\left(\xi_sr\right)+D_sK_0\left(\xi_sr\right)+T_s+q_m/\eta_b, & \text{for subcutis}\\ B_dI_0\left(\xi_dr\right)+D_dK_0\left(\xi_dr\right)+T_s+q_m/\eta_b, & \text{for dermis}\\ -\frac{q_m}{4\lambda_e}r^2+B_e\ln r+D_e, & \text{for epidermis}\end{cases} \tag{3}$$

where $\eta_b=\rho_b c_b\omega_b$, $\xi_i=\sqrt{\eta_b/\lambda_i}$, and the subscript $i=s$, d, and e represents the quantities of subcutis, dermis, and epidermis, respectively. $I_k(r)$ and $K_k(r)$ are, respectively, the modified Bessel functions of the first and second kind with kth order. The constants B_i and D_i can be determined by the temperature boundary conditions $T\left(r_s\right)=T_s$, $T\left(r_d\right)=T_d$, $T\left(r_e\right)=T_e$, and $T\left(r_c\right)=T_c$. For the sake of paper conciseness, these constants are provided in Appendix A.

Temperature Field for WATEG

It is noteworthy that the surface temperatures of human skin and flexible substrate, despite being in physical contact, may not necessarily be equal due to the presence of contact thermal resistance caused by the microscopic surface roughness on both contact surfaces. In this study, the semi-analytical model proposed by Bahrami et al.[22] is employed to characterize this contact thermal resistance. This resistance is directly proportional to the average thermal conductivity (κ_s), the average surface roughness slope (Δa), and the contact pressure (P_{TC}). Conversely, it is inversely proportional to the average surface roughness (ε) and the microhardness of the softer material (H_{TC}). The estimated contact thermal conductance can be expressed as follows:[22]

$$h_{TC}=1.25\kappa_s\frac{\Delta a}{\varepsilon}\left(\frac{P_{TC}}{H_{TC}}\right)^{0.95} \tag{4}$$

where the exponent 0.95 is the correction factor, and $\kappa_s=2\lambda_e\lambda_{\mathrm{TEG}}/\left(\lambda_e+\lambda_{\mathrm{TEG}}\right)$. Based on the examination of rough surface microgeometry, surface roughness can be depicted as shallow valleys and hills with small slopes, and the asperities exhibit spherical shapes at their summits. A commonly employed approach is to simplify the interaction between two Gaussian rough surfaces by replacing it with the contact between a flat plane and a randomly rough surface that possesses average surface characteristics.[22] Therefore, the average surface roughness slope Δa and the average surface roughness ε can be calculated as: $\Delta a=\sqrt{\Delta a_s^2+\Delta a_{\mathrm{TEG}}^2}$ and $\varepsilon=\sqrt{\varepsilon_s^2+\varepsilon_{\mathrm{TEG}}^2}$, where Δa_s and ε_s represent the surface asperity slope and surface roughness of the epidermis, respectively, while λ_{TEG}, Δa_{TEG}, and ε_{TEG} represent the thermal conductivity, surface asperity slope, and surface roughness of the flexible substrate of the WATEG, respectively.

The impact of contact thermal resistance at the epidermis/substrate interface can be accounted for in the heat transport analysis of the flexible substrate by defining an effective thermal conductivity λ_c, which is given by

$$\lambda_c=\frac{\lambda_e h_{TC}r_e\ln\left(r_1/r_e\right)}{\lambda_e+h_{TC}r_e\ln\left(r_1/r_e\right)} \tag{5}$$

where λ_e is the thermal conductivity of the flexible substrate. The temperature distribution within the flexible substrate is governed by the equation $\frac{\mathrm{d}^2T}{\mathrm{d}r^2}+\frac{1}{r}\frac{\mathrm{d}T}{\mathrm{d}r}=0$, with the following boundary conditions of $T\left(r_c\right)=T_c$ and $T\left(r_1\right)=T_1$. The solution for the temperature field in the flexible substrate is determined as:

$$T(r)=\frac{T_1-T_c}{\ln r_1-\ln r_c}\ln r+\frac{T_c\ln r_1-T_1\ln r_c}{\ln r_1-\ln r_c} \tag{6}$$

Similarly, the influence of the heat sink at the cold side of the WATEG can also be incorporated into the heat transfer of the encapsulation layer. The temperature field within the encapsulation layer is obtained by solving the heat transfer equation and applying the boundary condition of $T\left(r_2\right)=T_2$ and heat convection at the heat sink, given by $Q\left(r_a\right)=h_fA\left(r_a\right)\left[T\left(r_a\right)-T_a\right]$, where h_f is the convective heat transfer coefficient between the heat sink and ambient surroundings. The solution has the form of:

$$T(r)=\frac{T_2-T_a}{\ln r_2-\ln r_a-\lambda_{\mathrm{en}}/\left(h_fr_a\right)}\ln r+\frac{T_a\ln r_2-T_2\left[\ln r_a+\lambda_{\mathrm{en}}/\left(h_fr_a\right)\right]}{\ln r_2-\ln r_a-\lambda_{\mathrm{en}}/\left(h_fr_a\right)} \tag{7}$$

where λ_{en} is the thermal conductivity of the encapsulation layer.

The temperature field for the composite material layer consisting of thermoelectric legs and fill material satisfies the following heat transfer equation:

$$\lambda_{\text{eff}}\frac{\mathrm{d}^2T}{\mathrm{d}r^2}+\lambda_{\text{eff}}\frac{1}{r}\frac{\mathrm{d}T}{\mathrm{d}r}+q_g=0 \tag{8}$$

where λ_{eff} is the effective thermal conductivity taking into account the effect of thermoelectric legs and fill material, and can be calculated as:

$$\lambda_{\text{eff}}=\lambda_pF+\lambda_{\text{fm}}(1-F) \tag{9}$$

since the thermal resistance of the thermoelectric legs and that of the fill material are in parallel, where λ_p and λ_{fm} represent the thermal conductivities of P-type thermoelectric leg and fill material, respectively. The fill factor is defined as $F=(A_p+A_n)/A$, which denotes the area ratio of thermoelectric legs to the WATEG, where $A_p(r)=A_n(r)=r\theta_p\delta_p$ and $A(r)=r\theta\delta$ are the sectional areas of the P-type (N-type) leg and the WATEG, respectively. The last term in Eq. 8 is the Joule heat in thermoelectric legs and can be expressed as $q_g=j^2/\sigma_p+j^2/\sigma_n$, where j is the current density through the thermoelectric legs, σ_p and σ_n are the electric conductivity of P- and N-type thermoelectric legs, respectively. The temperature field for the composite material layer is obtained as:

$$T(r)=C_0(\ln r)^2+B_1\ln r+D_1 \tag{10}$$

where the constants C_0, B_1, and D_1 can be determined by the boundary conditions of $T(r_1)=T_1, T(r_2)=T_2$, and the governing Eq. 8, and given as

$$C_0=-\frac{I^2R}{2\lambda_{eff}\theta\delta\left[\ln r_2-\ln r_1\right]} \tag{11a}$$

$$B_1=\frac{T_1-T_2-C_0\left[(\ln r_1)^2-(\ln r_2)^2\right]}{\ln r_1-\ln r_2} \tag{11b}$$

$$D_1=\frac{T_2\ln r_1-T_1\ln r_2}{\ln r_1-\ln r_2}+C_0\ln r_1\ln r_2 \tag{11c}$$

where $R=R_p+R_n=2\frac{\ln(r_2/r_1)}{\sigma_p\theta_p\delta_p}$ is the internal electric resistance of the WATEG, and I is the electric current flowing through the WATEG.

Using Eqs. 2 and 10, and taking into account the Peltier heat at the junctions of thermoelectric legs, the heat flows at the inner and outer boundaries of the composite material layer are given by:

$$Q(r_1)=\alpha IT_1+K_{\text{eff}}(T_1-T_2)-\tfrac{1}{2}I^2R \tag{12a}$$

$$Q(r_2)=\alpha IT_2+K_{\text{eff}}(T_1-T_2)+\tfrac{1}{2}I^2R \tag{12b}$$

where $\alpha=\alpha_p-\alpha_n$ is the Seebeck coefficient, and $K_{eff}=\frac{\lambda_{eff}\theta\delta}{\ln(r_2/r_1)}$ is the effective thermal conductance of composite material layer. According to the principle of energy conservation, the heat flow should be continuous at the interfaces of the subcutis/dermis, dermis/epidermis, epidermis/substrate, substrate/thermoelectric composite layer, and thermoelectric composite layer/encapsulation layer. By utilizing the continuity conditions at these interfaces, the temperatures T_1 and T_2 can be obtained as follows:

$$T_1=\frac{-K_{\text{eff}}K_aT_a+(\alpha I-2K_{\text{eff}}-K_a)\frac{I^2R}{2}+\gamma_1K_c\frac{\Omega_s}{\Omega_c}T_s}{K_{\text{eff}}^2+\gamma_1\gamma_2} \tag{13a}$$

$$T_2=-\frac{\gamma_2K_aT_a+\left(\alpha I+2K_{\text{eff}}+K_c+\frac{K_c^2}{K_e\Omega_c}\right)\frac{I^2R}{2}+\frac{\Omega_s}{\Omega_c}K_{\text{eff}}K_cT_s}{K_{\text{eff}}^2+\gamma_1\gamma_2} \tag{13b}$$

where $K_c=\frac{\lambda_c\theta\delta}{\ln(r_1/r_c)}$ and $K_a=\frac{\lambda_{en}\theta\delta}{\ln(r_a/r_2)+\lambda_{en}/(h_fr_a)}$ are the thermal conductance of flexible substrate (including skin/WATEG interface) and encapsulation layer (including heat sink), respectively. The constants γ_1, γ_2, Ω_s, and Ω_c, as well as the temperatures T_d, T_e, and T_c are provided in Appendix B.

Energy Conversion Performance of the WATEG

The power output, denoted as P_{out}, of the WATEG can be estimated using the following equations. Firstly, it can be calculated as the difference between the heat flow rates at the hot and cold of the composite material layer and given by:

$$P_{\text{out}}=Q(r_1)-Q(r_2)=\alpha I(T_1-T_2)-I^2R \tag{14}$$

Alternatively, the power output can also be calculated as:

$$P_{\text{out}}=I^2R_L \tag{15}$$

where R_L is the imposed electric resistance. Combining Eqs. 14 and 15, the equation for current is obtained as:

$$I=\frac{\alpha(T_1-T_2)}{R+R_L} \tag{16}$$

By substituting Eq. (13) into Eq. 16, the cubic equation of electric current is given by:

$$G_3I^3+G_2I^2+G_1I+G_0=0 \tag{17}$$

where the coefficients G_3, G_2, G_1, and G_0 are given as follows:

$$G_3=\alpha^2R_L \tag{18a}$$

$$G_2 = \alpha\left(K_c + \frac{K_c^2}{K_e\Omega_c} - K_a\right)\left(\frac{R}{2} + R_L\right) \tag{18b}$$

$$G_1 = -\alpha^2\left(K_aT_a + K_c\frac{\Omega_s}{\Omega_c}T_s\right) - \left[K_c\left(K_{\text{eff}} + K_a\right)\left(1 + \frac{K_c}{K_e\Omega_c}\right) + K_{\text{eff}}K_a\right]\left(R + R_L\right) \tag{18c}$$

$$G_0 = \alpha K_aK_c\left[\frac{\Omega_s}{\Omega_c}T_s - \left(1 + \frac{K_c}{K_e\Omega_c}\right)T_a\right] \tag{18d}$$

Equation (17) has three solutions that can be found in the mathematical handbook. The physical acceptable exact solution for Eq. 17 is given as:

$$I = -\frac{G_2}{3G_3} + \omega^2\sqrt[3]{-\frac{q}{2} + \sqrt{\left(\frac{q}{2}\right)^2 + \left(\frac{p}{3}\right)^3}} + \omega\sqrt[3]{-\frac{q}{2} - \sqrt{\left(\frac{q}{2}\right)^2 + \left(\frac{p}{3}\right)^3}} \tag{19}$$

where $\omega = \frac{-1+\sqrt{3}i}{2}$, $p = \frac{G_1}{G_3} - \frac{G_2^2}{3G_3^2}$, $q = \frac{G_0}{G_3} + \frac{2G_2^2}{27G_3^3} - \frac{G_1G_2}{3G_3^2}$. The power output of the WATEG can then be calculated by Eq. 15.

Numerical Results and Discussion

In this section, the influence of human skin, geometrical dimensions of WATEG, and thermal boundary conditions on the performance of the WATEG is investigated through numerical examples. The PDMS (polydimethylsiloxane) and Bi_2Te_3 are selected as the fill material and thermoelectric material, respectively. The materials properties and dimensions for the skin tissue and WATEG used are provided in Table I, unless otherwise stated. It is noted that a more reasonable range for the natural convective heat transfer coefficient of air (h_f) is typically between 6 W/m^{2}K and 10 W/m^{2}K.[26] However, when the WATEG is worn on the human body, the effective h_f may be significantly enhanced due to its movement along with the human body, such as walking, running, and jumping. Therefore, in this paper, the convective heat transfer coefficient, taking into account the convection caused by the average motion of the wearer in still air, is determined to be 25 W/m^{2}K. Additionally, the maximum value for the forced convective heat transfer coefficient is noted as 200W/m^{2}K.[26] The metabolic heat generation in the skin tissue is given as $q_m = 368$W/m^3.[23] The thicknesses of the thermoelectric leg and WATEG are 1 mm and 2 mm, respectively. The angle in the direction of the circumference for the P-type thermoelectric leg is $\theta_p = 0.03$rad, and the angle of WATEG is determined by the definition of the fill factor and the angle θ_p.

Table I Material parameters used in this article[10,11,23–25]

Material	Parameter	Value	Height (mm)
Subcutis	Body core temperature T_S (K)	310	4.4
	Thermal conductivity λ_s (W/mK)	0.185	
Dermis	Thermal conductivity λ_d (W/mK)	0.445	1.5
Epidermis	Thermal conductivity λ_e (W/mK)	0.235	0.1
	Surface roughness ε_s (μm)	21.69	
	Surface asperity slope Δa_s (rad)	0.3	
	Microhardness H_{TC} (MPa)	0.1225	
	Contact pressure P_{TC} (kPa)	0.5	
Blood	Blood perfusion rate ω_b (mL/(mLs))	0.05	–
	Density ρ_b (kg/m^3)	1060	
	Specific heat c_b (J/kgK)	3770	
Encapsulating and substrate layer (silicone rubber)	Thermal conductivity λ_{en} (W/mK)	4.0	0.5
	Surface roughness ε_{TEG} (μm)	1	
	Surface roughness slope Δa_{TEG} (rad)	0.009	
Ambient air	Convection coefficient h_f (W/m^{2}K)	25	–
	Ambient temperature T_a (K)	288	
Fill material (PDMS)	Thermal conductivity λ_{fm} (W/mK)	0.27	2
Thermoelectric legs (Bi_2Te_3)	Fill factor F	0.2	2
	Seebeck coefficient α_p (μV/K)	200	
	Electric conductivity σ_P (S/m)	11000	
	Thermal conductivity λ_P (W/mK)	1.6	

The Influence of Human Skin and Imposed Load Resistance

The variations in human skin effects, including metabolic heat generation and heat exchange induced by the blood perfusion, and the imposed electric resistance (R_L) on the temperature drop (ΔT) across the thermoelectric legs and the power density (P_m) of the WATEG are illustrated in Fig. 2. The power density is defined as the ratio of the power out to the cross-sectional area of the mid-plane of the WATEG, denoted as, $P_m = P_{out}/A_m$, where $A_m = (r_1 + r_2)\theta\delta/2$. It is observed that the temperature drop increases with the increasing values of imposed load resistance. There exists an optimal R_L, referred to as the matched load resistance, corresponding to the maximum power density. For typical TEGs with constant temperature boundary conditions at the hot and cold ends, the ratio of matched electrical load resistance to the internal resistance R_L/R is 1 for achieving maximum power output and $\sqrt{1+ZT}$ for achieving maximum energy conversion efficiency, where ZT is the figure of merit of the TEG. However, when constant heat flow boundary conditions are applied, the optimal ratio of R_L/R becomes $\sqrt{1+ZT}$ for both maximum power and maximum energy conversion efficiency.[27] Notably, the matched load resistance for WATEG, taking into account the human skin effect, is significantly larger than the classical values, particularly in this study, the value becomes $R_L/R = 1.4674$. Furthermore, it is worth mentioning that the influence of metabolic heat generation within the skin tissue on the power density of the WATEG is negligible and can be disregarded. However, the impact of blood perfusion is substantial and should be considered when accurately predicting the performance of WATEGs for configuration optimization.

The exact solution for the current in Eq. 17 is complex and not suitable for practical engineering applications. However, for a well-designed WTEG, it has been found that the values of aI^3 and bI^2 are significantly smaller than those of cI and d in Eq. 17.[11,17] This conclusion also holds for WATEG. By neglecting aI^3 and bI^2, Eq. 17 can be simplified to $cI + d = 0$, and the linear solution for the electric current I can be expressed as:

$$I = \frac{\alpha K_a K_c \left[\frac{\Omega_s}{\Omega_c} T_s - \left(1 + \frac{K_c}{K_e \Omega_c}\right) T_a\right]}{\alpha^2 \left(K_a T_a + K_c \frac{\Omega_s}{\Omega_c} T_s\right) + \left[K_c \left(K_{\text{eff}} + K_a\right)\left(1 + \frac{K_c}{K_e \Omega_c}\right) + K_{\text{eff}} K_a\right](R + R_L)} \tag{20}$$

The comparison of numerical results of the current I between the exact solution in Eq. 19 and the linear simplified solution in Eq. 20 is illustrated in Fig. 3. We can see that the differences between the two solutions are negligible even when the imposed electric resistance varies over a wide range, with a maximum error of less than 0.01%.

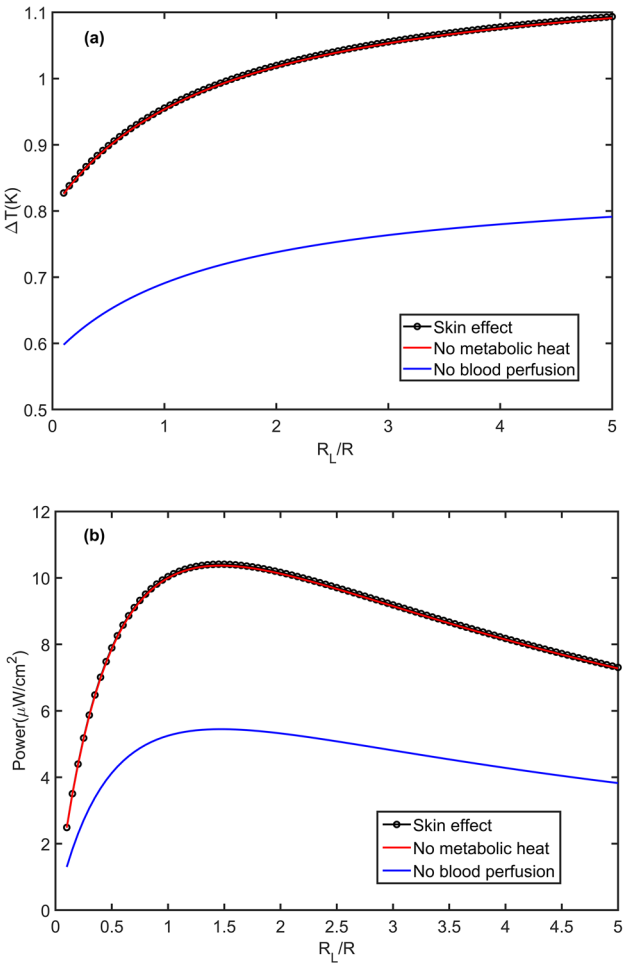

Fig. 2 Effects of human skin and imposed load resistance on the performance of WATEG. (a) Temperature drop across the thermoelectric legs. (b) Power density.

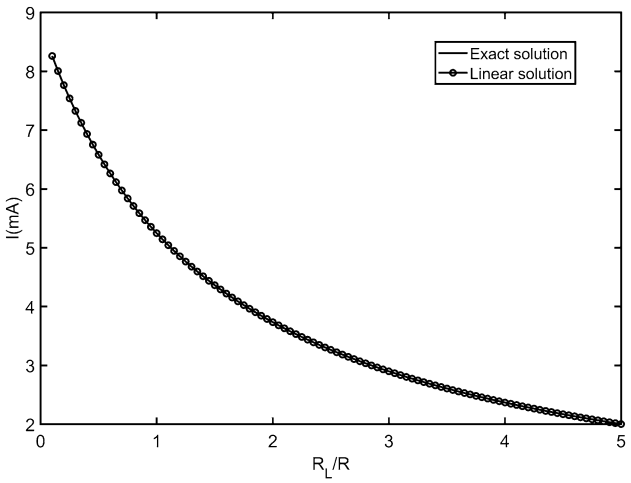

Fig. 3 Comparison of exact solution and linear simplified solution for the electric current flowing through the WATEG.

The linear simplified solution achieves a very high level of accuracy. Furthermore, the power output of the WATEG can be obtained by substituting Eq. 20 into Eq. 15 and solving for $dP_{out}/dR_L = 0$, which allows for the determination of the matched load resistance R_L in closed-form. The expression for matched R_L has the following form:

$$\frac{R_L}{R} = 1 + Z\frac{F}{F + (1-F)\lambda_{fm}/\lambda_p} \times \frac{K_a T_a + K_c \frac{\Omega_s}{\Omega_c} T_s}{K_a + K_c\left(1 + \frac{K_c}{K_e \Omega_c}\right) + K_a K_c\left(1 + \frac{K_c}{K_e \Omega_c}\right)/K_{\text{eff}}} \quad (21)$$

From Eq. 21, it is evident that the matched load resistance depends not only on the internal resistance, figure of merit, and fill factor of the WATEG, but also on its configuration dimensions, thermal properties of human skin, and boundary conditions. The matched R_L/R calculated using Eq. 21 is 1.4675, which is consistent with the accurate numerical result.

The Influence of Fill Factor and Fill Material

Figure 4 illustrates the variations in temperature drop across the thermoelectric legs and power density of the WATEG in relation to the fill factor and the thermal conductivity of the fill material. Generally, the thermal conductivity of thermoelectric legs is much larger than that of the fill material, as shown in Table I. Specifically, fill materials with low thermal conductivity are capable of maintaining the temperature gradient between the hot and cold sides of thermoelectric legs, as depicted in Fig. 4a. As a result, the performance of the WATEG can be effectively enhanced as the fill factor decreases. However, as the fill factor decreases to a certain extent, the number of thermoelectric legs capable of undergoing thermoelectric conversion becomes limited, leading to a decline in the performance of the WATEG in converting heat energy into electricity. In the extreme case where the fill factor is zero, the power output naturally becomes zero as well, even if the temperature drop takes the maximum value in this case. Thus, the fill factor of the WATEG possesses an optimal value, as demonstrated in Fig. 4b. Four types of fill materials are assumed to be used in numerical analysis, namely vacuum, air, porous PDMS (half air and half PDMS), and PDMS with the thermal conductivities λ_{fm} of 0 W/mK, 0.025 W/mK, 0.135 W/mK, and 0.27 W/mK, respectively. It can be observed that the optimal fill factor, corresponding to maximum power density of the WATEG, increases as the thermal conductivity of the fill material increases. Specifically, the optimal fill factors are 0.0141, 0.0260, 0.0819, and 0.1599 for the λ_{fm} values of 0 W/mK, 0.025 W/mK, 0.135 W/mK, and 0.27 W/mK, respectively.

On the other hand, another crucial function of the fill material is to withstand the large deformation and ensure the mechanical reliability of the WATEG. Therefore, the fill factor generally should not be less than 0.2.[9] This is because the optimal fill factor represents a trade-off between energy conversion performance and the structural stability of the WATEG, especially taking the thermal properties of the fill material into consideration.

The Influence of the Height of Thermoelectric Legs

Figure 5 depicts the variations in temperature drop across the thermoelectric legs and power density of the WATEG as a function of the height of thermoelectric legs, where the parameters H_P and H are the height of the thermoelectric

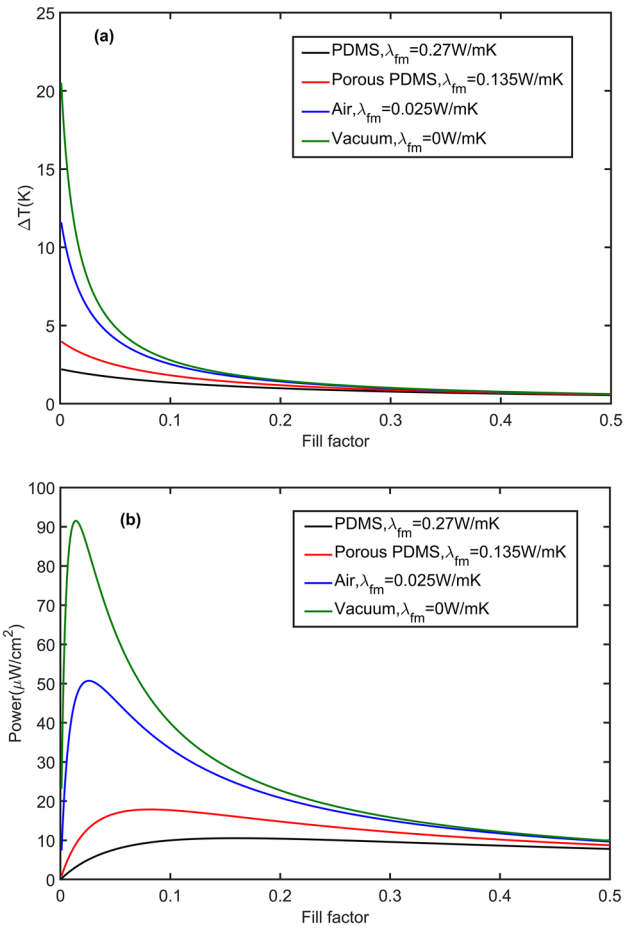

Fig. 4 Effects of fill factor and thermal conductivity of fill material on the performance of WATEG. (a) Temperature drop across the thermoelectric legs. (b) Power density.

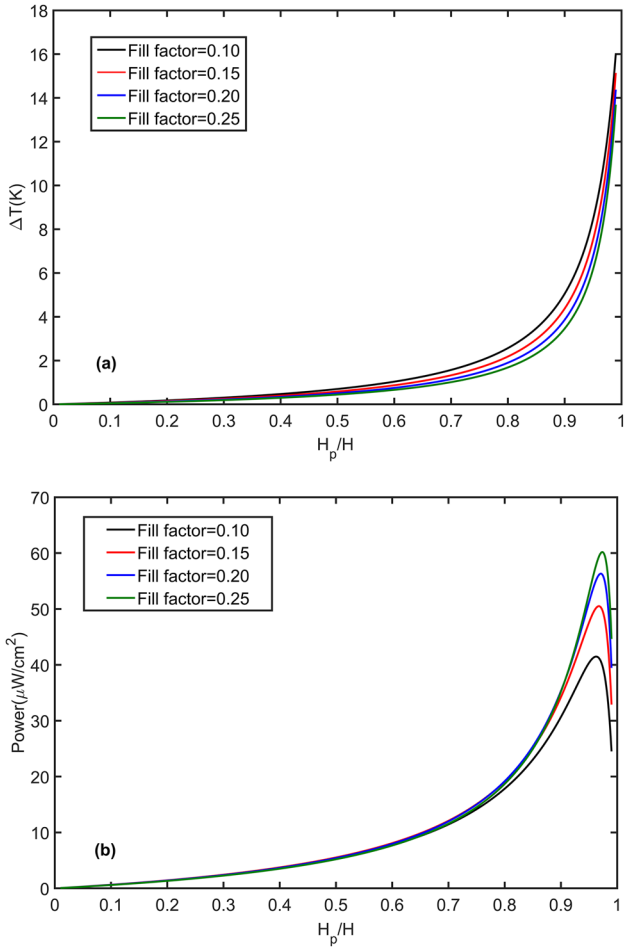

Fig. 5 Effects of the height of thermoelectric legs and fill factor on the performance of WATEG. (a) Temperature drop across the thermoelectric legs. (b) Power density.

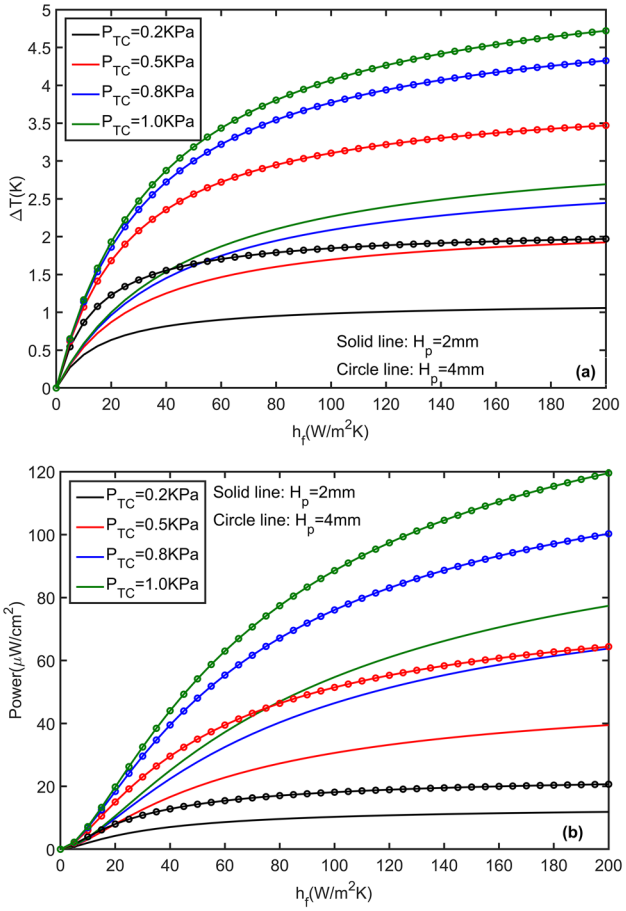

Fig. 6 Effects of the contact thermal resistance at the skin/substrate interface and thermal boundary condition on the performance of the WATEG. (a) Temperature drop across the thermoelectric legs. (b) Power density.

legs and WATEG, respectively. The height of the thermoelectric legs plays an essential role in determining the thermal resistance of the WATEG, and the temperature drop and the power density exhibit a rapid increasing trend as the ratio of H_P/H increases. The optimal height ratios H_P/H are found to be 0.9627, 0.9676, 0.9711, and 0.9737 for fill factors of 0.10, 0.15, 0.20, and 0.25, respectively, nearly approaching unity. However, achieving these optimal height ratios in practical applications present challenges with regard to wearable performance and mechanical reliability.[28,29] For instance, if the height of the flexible substrate and that of the encapsulation layer are both 0.5 mm, the optimal H_P would be 33.60 mm for a fill factor of 0.20. Therefore, in order to maximize the power output of the WATEG while ensuring wearability, it is crucial to design the thermoelectric legs with the longest possible height.

The Influence of Contact Thermal Resistance at the Skin/Substrate Interface and Thermal Boundary Condition

The performance of the WATEG is presented in Fig. 6, as a function of contact thermal resistance at the skin/substrate interface and thermal boundary condition. Two different heights of the thermoelectric legs, namely 2 mm and 4 mm, are considered. Both the temperature drop and power density increase with increasing values of contact pressure and convective heat transfer coefficient at the heat sink. It is noteworthy that the contact thermal resistance at the interface between human skin and WATEG is primarily influenced by the surface characteristics of the skin, flexible substrate, and contact pressure. Although the physical properties of human skin and flexible substrate are not easily optimized, the contact thermal resistance can be significantly reduced by increasing the contact pressure. This is because the heat transfer at the skin/substrate interface is predominantly

conducted through the actual contact area, which can be increased by the soft nature of human skin under higher contact pressure. However, the contact pressure should not be too high to avoid discomfort to the human body. For reference, typical contact pressure for tight-fitting clothing ranges from 0.5 kPa to 0.8 kPa.

Conclusions

In conclusion, this paper presents an analytical model for investigating the energy conversion performance of the WATEG harvesting human body heat. The human skin is modeled as a cylindrical multilayer structure comprising subcutis, dermis, and epidermis, taking into account the metabolic heat generation and blood perfusion within the skin tissue based on the Pennes bioheat transfer equation. It is found that accurate estimation of WATEG performance requires consideration of the influence of heat exchange induced by blood perfusion. The contact thermal resistance at the skin/WATEG interface significantly weakens the power output of the WATEG, but this effect can be mitigated by appropriately increasing the contact pressure. Additionally, a closed-form expression for the matched load resistance is provided, and the optimal fill factor and optimal height of thermoelectric legs corresponding to maximum power density are determined. The theoretical model developed in this paper can serve as a valuable tool for configuration optimization and design of actual WATEG devices.

Appendix A

The constants B_i and D_i ($i = s, d$ and e):

$$B_s = -\frac{\frac{q_m}{\eta_b}K_0(\xi_s r_d)+\left(T_d-T_s-\frac{q_m}{\eta_b}\right)K_0(\xi_s r_s)}{I_0(\xi_s r_s)K_0(\xi_s r_d)-I_0(\xi_s r_d)K_0(\xi_s r_s)} \tag{A1}$$

$$D_s = \frac{\frac{q_m}{\eta_b}I_0(\xi_s r_d)+\left(T_d-T_s-\frac{q_m}{\eta_b}\right)I_0(\xi_s r_s)}{I_0(\xi_s r_s)K_0(\xi_s r_d)-I_0(\xi_s r_d)K_0(\xi_s r_s)} \tag{A2}$$

$$B_d = \frac{T_d K_0(\xi_d r_e)-T_e K_0(\xi_d r_d)+\left(T_s+\frac{q_m}{\eta_b}\right)[K_0(\xi_d r_d)-K_0(\xi_d r_e)]}{I_0(\xi_d r_d)K_0(\xi_d r_e)-I_0(\xi_d r_e)K_0(\xi_d r_d)} \tag{A3}$$

$$D_d = \frac{T_d I_0(\xi_d r_e)-T_e I_0(\xi_d r_d)+\left(T_s+\frac{q_m}{\eta_b}\right)[I_0(\xi_d r_d)-I_0(\xi_d r_e)]}{I_0(\xi_d r_d)K_0(\xi_d r_e)-I_0(\xi_d r_e)K_0(\xi_d r_d)} \tag{A4}$$

$$B_e = \frac{T_e-T_c-\frac{q_m}{4\lambda_e}\left(r_c^2-r_e^2\right)}{\ln r_e-\ln r_c} \tag{A5}$$

$$D_e = -\frac{T_e \ln r_c-T_c \ln r_e+\frac{q_m}{4\lambda_e}\left(r_e^2 \ln r_c-r_c^2 \ln r_e\right)}{\ln r_e-\ln r_c} \tag{A6}$$

where $K_s = \frac{\lambda_s \theta \delta}{\ln(r_d/r_s)}$, $K_d = \frac{\lambda_d \theta \delta}{\ln(r_e/r_d)}$, $K_e = \frac{\lambda_e \theta \delta}{\ln(r_c/r_e)}$ are the thermal conductances of subcutis, dermis, and epidermis, respectively.

Appendix B

The temperatures T_d, T_e and T_c, and the constants γ_1, γ_2, Ω_c and Ω_s:

$$T_d = \frac{\mu_{s1}T_s-\mu_{e1}T_e}{\mu_{d1}} \tag{B1}$$

$$T_e = \frac{\mu_{s2}T_s-\mu_{c1}T_c-\mu_{d2}T_d}{\mu_{e2}} \tag{B2}$$

$$T_c = -\frac{K_c}{K_e\Omega_c}T_1 + \frac{\Omega_s}{\Omega_c}T_s \tag{B3}$$

$$\gamma_1 = \alpha I - K_{eff} - K_a \tag{B4}$$

$$\gamma_2 = \alpha I + K_{\text{eff}} + K_c + \frac{K_c^2}{K_e\Omega_c} \tag{B5}$$

$$\Omega_c = \frac{\mu_{d1}\mu_{c1}}{\mu_{e1}\mu_{d2}-\mu_{e2}\mu_{d1}} - 1 - \frac{K_c}{K_e} \tag{B6}$$

$$\Omega_s = \frac{\mu_m}{T_s} - \frac{\mu_{d2}\mu_{s1}-\mu_{d1}\mu_{s2}}{\mu_{e1}\mu_{d2}-\mu_{e2}\mu_{d1}} \tag{B7}$$

with

$$\mu_{d1} = \frac{I_1(\xi_s r_d)K_0(\xi_s r_s)+I_0(\xi_s r_s)K_1(\xi_s r_d)}{I_0(\xi_s r_s)K_0(\xi_s r_d)-I_0(\xi_s r_d)K_0(\xi_s r_s)} + \mu_{e1} \tag{B8}$$

$$\mu_{e1} = \frac{K_d\xi_d \ln\frac{r_e}{r_d}}{K_s\xi_s \ln\frac{r_d}{r_s}} \frac{I_1(\xi_d r_d)K_0(\xi_d r_d)+I_0(\xi_d r_d)K_1(\xi_d r_d)}{I_0(\xi_d r_d)K_0(\xi_d r_e)-I_0(\xi_d r_e)K_0(\xi_d r_d)} \tag{B9}$$

$$\mu_{s1} = \frac{\mu_{s11}\left(1+\frac{q_m}{\eta_b T_s}\right)-\mu_{s12}\frac{q_m}{\eta_b T_s}}{\mu_{s14}} - \frac{K_d\xi_d \ln\frac{r_e}{r_d}}{K_s\xi_s \ln\frac{r_d}{r_s}} \cdot \frac{\mu_{s13}}{\mu_{s15}} \tag{B10}$$

$$\mu_{s11} = I_1(\xi_s r_d)K_0(\xi_s r_s) + I_0(\xi_s r_s)K_1(\xi_s r_d) \tag{B11}$$

$$\mu_{s12} = I_1(\xi_s r_d)K_0(\xi_s r_d) + I_0(\xi_s r_d)K_1(\xi_s r_d) \tag{B12}$$

$$\begin{aligned}\mu_{s13} =& I_1(\xi_d r_d)[K_0(\xi_d r_d) - K_0(\xi_d r_e)] \\ &+ K_1(\xi_d r_d)\left[I_0(\xi_d r_d) - I_0(\xi_d r_e)\right]\end{aligned} \tag{B13}$$

$$\mu_{s14} = I_0(\xi_s r_s)K_0(\xi_s r_d) - I_0(\xi_s r_d)K_0(\xi_s r_s) \tag{B14}$$

$$\mu_{s15} = I_0(\xi_d r_d)K_0(\xi_d r_e) - I_0(\xi_d r_e)K_0(\xi_d r_d) \tag{B15}$$

$$\mu_{d2} = \frac{I_1(\xi_d r_e)K_0(\xi_d r_e)+I_0(\xi_d r_e)K_1(\xi_d r_e)}{I_0(\xi_d r_d)K_0(\xi_d r_e)-I_0(\xi_d r_e)K_0(\xi_d r_d)} \tag{B16}$$

$$\mu_{e2} = -\frac{I_1(\xi_d r_e)K_0(\xi_d r_d)+I_0(\xi_d r_e)K_1(\xi_d r_e)}{I_0(\xi_d r_d)K_0(\xi_d r_e)-I_0(\xi_d r_e)K_0(\xi_d r_d)} + \mu_{c1} \tag{B17}$$

$$\mu_{c1} = \frac{K_e}{K_d \xi_d r_e \ln\frac{r_e}{r_d}} \tag{B18}$$

$$\mu_{s2} = \frac{K_e q_m r_e \ln\frac{r_c}{r_e}}{2\lambda_e K_d \xi_d T_s \ln\frac{r_e}{r_d}} + \frac{K_e q_m (r_c^2 - r_e^2)}{4\lambda_e K_d \xi_d r_e T_s \ln\frac{r_e}{r_d}} - \left(1 + \frac{q_m}{\eta_b T_s}\right)\mu_{s21} \tag{B19}$$

$$\mu_{s21} = \frac{I_1(\xi_d r_e)\left[K_0(\xi_d r_d)-K_0(\xi_d r_e)+K_1(\xi_d r_e)\right]\left[I_0(\xi_d r_d)-I_0(\xi_d r_e)\right]}{I_0(\xi_d r_d)K_0(\xi_d r_e)-I_0(\xi_d r_e)K_0(\xi_d r_d)} \tag{B20}$$

$$\mu_m = \frac{q_m}{4\lambda_e}\left[r_c^2\left(1 - 2\ln\frac{r_c}{r_e}\right) - r_e^2\right] \tag{B21}$$

Acknowledgments The research was supported by the Natural Science Foundation of Zhejiang Province of China (LY21A020004), the Natural Science Foundation of Ningbo (2022J095), the Natural Science Youth Foundation of Henan Province (232300420336), the Key University Scientific Research Project of Henan Province (22A610007), and the Special Scientific Research Fund Project of Cultivating Master Graduates of Huangshan University (hsxyssd008).

Conflict of interest The authors declare that they have no financial interests or personal relationships with other people or organizations that can inappropriately influence the work reported in this paper.

References

1. X. Wang, Z. Liu, and T. Zhang, Flexible sensing electronics for wearable/attachable health monitoring. *Small* 13(25), 1602790 (2017).
2. T.Q. Trung and N.-E. Lee, Flexible and stretchable physical sensor integrated platforms for wearable human-activity monitoring and personal healthcare. *Adv. Mater.* 28(22), 4338–4372 (2016).
3. A.S. Dahiya, J. Thireau, J. Boudaden, S. Lal, U. Gulzar, Y. Zhang, T. Gil, N. Azemard, P. Ramm, T. Kiessling, C. O'Murchu, F. Sebelius, J. Tilly, C. Glynn, S. Geary, C. O'Dwyer, K.M. Razeeb, A. Lacampagne, B. Charlot, and A. Todri-Sanial, Review-energy autonomous wearable sensors for smart healthcare: a review. *J. Electrochem. Soc.* 167(3), 037516 (2019).
4. W. Ren, Y. Sun, D. Zhao, A. Aili, S. Zhang, C. Shi, J. Zhang, H. Geng, J. Zhang, L. Zhang, J. Xiao, and R. Yang, High-performance wearable thermoelectric generator with self-healing, recycling, and Lego-like reconfiguring capabilities. *Sci. Adv.* 7(7), eabe0586 (2021).
5. A. Nozariasbmarz, H. Collins, K. Dsouza, M.H. Polash, M. Hosseini, M. Hyland, J. Liu, A. Malhotra, F.M. Ortiz, F. Mohaddes, V.P. Ramesh, Y. Sargolzaeiaval, N. Snouwaert, M.C. Özturk, and D. Vashaee, Review of wearable thermoelectric energy harvesting: from body temperature to electronic systems. *Appl. Energy* 258, 114069 (2020).
6. P. Kolarsick, M.A. Kolarsick, and C. Goodwin, Anatomy and Physiology of the Skin. *J. Dermatol. Nurs. Assoc.* 3(4), 203 (2011).
7. N. Djongyang, R. Tchinda, and D. Njomo, Thermal comfort: a review paper. *Renew. Sust. Energy. Rev.* 14(9), 2626–2640 (2010).
8. G. Kelly, Body temperature variability (Part 1): a review of the history of body temperature and its variability due to site selection, biological rhythms, fitness, and aging. *Altern. Med. Rev.* 11(4), 278 (2006).
9. F. Suarez, A. Nozariasbmarz, D. Vashaee, and M.C. Öztürk, Designing thermoelectric generators for self-powered wearable electronics. *Energy Environ. Sci.* 9, 2099–2113 (2016).
10. D. Wijethunge, D. Kim, and W. Kim, Simplified human thermoregulatory model for designing wearable thermoelectric devices. *J. Phys. D Appl. Phys.* 51, 055401 (2018).
11. A.B. Zhang, G.Y. Li, B.L. Wang, and J. Wang, A theoretical model for wearable thermoelectric generators considering the effect of human skin. *J. Electron. Mater.* 50, 1514–1526 (2021).
12. A.B. Zhang, D.D. Pang, B.L. Wang, and J. Wang, Dynamic responses of wearable thermoelectric generators used for skin waste heat harvesting. *Energy* 262, 125621 (2023).
13. F. Suarez, D.P. Parekh, C. Ladd, D. Vashaee, M.D. Dickey, and M.C. Öztürk, Flexible thermoelectric generator using bulk legs and liquid metal interconnects for wearable electronics. *Appl. Energy* 202, 736–745 (2017).
14. M.H. Jeong, K.C. Kim, J.S. Kim, and K.J. Choi, Operation of wearable thermoelectric generators using dual sources of heat and light. *Adv. Sci.* 9(12), 2104915 (2022).
15. Z.G. Shen, S.Y. Wu, and L. Xiao, Theoretical analysis on the performance of annular thermoelectric couple. *Energy Convers. Manag.* 89, 244–250 (2015).
16. S.C. Kaushik and S. Manikandan, The influence of Thomson effect in the energy and exergy efficiency of an annular thermoelectric generator. *Energy Convers. Manag.* 103, 200–207 (2015).
17. A.B. Zhang, B.L. Wang, D.D. Pang, L.W. He, J. Lou, J. Wang, and J.K. Du, Effects of interface layers on the performance of annular thermoelectric generators. *Energy* 147, 612–620 (2018).
18. A.B. Zhang, B.L. Wang, D.D. Pang, J.B. Chen, J. Wang, and J.K. Du, Influence of leg geometry configuration and contact resistance on the performance of annular thermoelectric generators. *Energy Convers. Manag.* 166, 337–342 (2018).
19. Z.F. Wen, Y. Sun, A.B. Zhang, B.L. Wang, J. Wang, and J.K. Du, Performance analysis of a segmented annular thermoelectric generator. *J. Electron. Mater.* 49, 4830–4842 (2020).
20. S.F. Fan and Y.W. Gao, Numerical analysis on the segmented annular thermoelectric generator for waste heat recovery. *Energy* 183, 35–47 (2019).
21. H.H. Pennes, Analysis of tissue and arterial blood temperatures in the resting human forearm. *J. Appl. Physiol.* 1, 93–122 (1948).
22. M. Bahrami, J.R. Culham, and M.M. Yovanavich, Modeling thermal contact resistance: a scale analysis approach. *J. Heat Transf.* 126, 896–905 (2004).
23. F. Xu, T.J. Lu, and K.A. Seffen, Biothermomechanics of skin tissues. *J. Mech. Phys. Solids* 56, 1852–1884 (2008).
24. Y.C. Wang, Y.G. Shi, D.Q. Mei, and Z.C. Chen, Wearable thermoelectric generator for harvesting heat on the curved human wrist. *Appl. Energy* 205, 710–719 (2017).
25. H.N. Ho and L.A. Jones, Modeling the thermal responses of the skin surface during hand-object interactions. *J. Biomech. Eng. T ASME* 130, 021005 (2008).
26. F.P. Incropera, D.P. DeWitt, T.L. Bergman, and A.S. Lavine, *Fundamentals of Heat and Mass Transfer*, 6th ed., (New York: Wiley, 1996).

27. M. Gao, New formulation of the theory of thermoelectric generators operating under constant heat flux. *Energ. Environ. Sci.* 15, 356–367 (2022).
28. A.B. Zhang, J. Lou, B.L. Wang, and J. Wang, A Griffith crack model in a generalized nonhomogeneous interlayer of bonded dissimilar half-planes. *J. Theort. Appl. Mech.* 61, 495–507 (2023).
29. A.B. Zhang and B.L. Wang, Temperature and electric potential fields of an interface crack in a layered thermoelectric or metal/thermoelectric material. *Int. J. Therm. Sci.* 104, 396–403 (2016).